EARTH'S CRYOSPHERE
SCIENTIFIC JOURNAL

Earth`s Cryosphere, 2019, vol. XXIII, No. 1, pp. 26–34 **http://earthcryosphere.ru/**

CRYOGENIC PROCESSES AND FORMATIONS

DOI: 10.21782/EC2541-9994-2019-1(26-34)

COASTAL DYNAMICS OF THE BERING SEA (LORINO SITE, CHUKCHI PENINSULA, RUSSIA)

A.A. Maslakov

Lomonosov Moscow State University, Faculty of Geography, Laboratory of Geoecology of the North, 1, Leninskie Gory, Moscow, 119991, Russia; alexey.maslakov@geogr.msu.ru

The study presents results of coastal retreat monitoring within a 750 m long remnant of a marine terrace near Lorino community, on the Bering Sea shore. The monitoring data are used to estimate the rate of coastal retreat (landward movement of bluff foot) as a function of coast parameters, and relative contributions of thermal abrasion and thermal denudation to coastal erosion and material loss. The retreat rates at the Lorino site vary both in time and in space: they were about nine times faster in 2014–2017 than in 1967–2014 (4.2 m/yr against 0.4 m/yr), while lateral variations have been controlled by coast parameters and mechanic strength of rocks exposed to wave action.

Thermal abrasion, thermal denudation, coastal dynamics, Lorino, Chukchi Peninsula, Bering Sea

INTRODUCTION

Climate change in the Arctic [*Pachauri and Meyer, 2014*], with warming of air and permafrost temperatures and the ensuing increase in seasonal thaw depth and decrease in ice richness [*Comiso et al., 2008; Barber et al., 2017; Romanovsky et al., 2017*], lead to progressive retreat of the Arctic coast [*Forbes, 2011; Overeem et al., 2011; AMAP, 2017*]. Coastal erosion has been markedly more rapid in recent years during the open water season from October to December, in the time of strongest winds in the eastern Russian Arctic [*Zimich, 2002; Atkinson, 2005*]. The lack of sea ice increases erosive effectiveness of winds and storms which would be minor upon an ice-covered coast. The acceleration of retreat rates was reported from many parts of the Arctic coast [*Lantuit and Pollard, 2008; Forbes, 2011; Kritsuk et al., 2014; Maslakov and Kraev, 2016; Pizhankova, 2016; Belova et al., 2017; Irrgang et al., 2018*]. The mean annual retreat was estimated to reach 0.5 m [*Lantuit et al., 2012*] from data of systematic field surveys and remote sensing that span <100,000 km or 25 % of the total Arctic coast length. However, its rates are as fast as 2.0 to 3.8 m/yr (depending on lithology) in the eastern part of the Russian Arctic coast composed of fine-grained ice-rich permafrost [*Grigoriev et al., 2006*].

Although estimates are available for mean rates of coastal retreat, the contributions of different natural agents, including surface processes, into the coastal dynamics remain poorly constrained [*Are, 2012*]. It is hard to evaluate the inputs of two main destructive processes of thermo-abrasion and thermo-denudation to the retreat of frozen coast, because of the present and future (predicted) instability of climate and hydrodynamics; due regard for the balance of sediment accumulation in the Artic shelf is another challenge.

This paper presents results of coastal retreat monitoring within a 750 m long remnant of a marine terrace near Lorino community, on the Bering Sea shore (eastern Chukchi Peninsula). The study addresses the relationship between the retreat rate and coast parameters, as well as relative contributions of thermo-abrasion and thermo-denudation to coastal erosion.

STUDY AREA

Lorino community (Fig. 1) is located in the eastern Chukchi Peninsula on the Bering Sea coast (Mechigmen Bay). It was first mentioned in historic accounts in the 16th century, and is currently one of largest communities in the peninsula [*Chukchi Municipal Area. www.chukotraion.ru*]. The study area is a low plateau composed of Mesozoids and surrounded by narrow fragments of coastal plains [*Parmuzin, 1968*]. The territory lies in the zone of Subarctic and Arctic maritime climate, with cloudy and cool summers (mean July air temperature: 8 to 10 °C) and long moderately cold winters (mean January air temperature: –24 to –26 °C) [*Kobysheva, 2001*]. The landscapes are typical tundra in river valleys and lichen tundra with bare hills on elevated landforms [*Isachenko, 1985*]. Permafrost is continuous and varies in thickness and temperatures, respectively, between

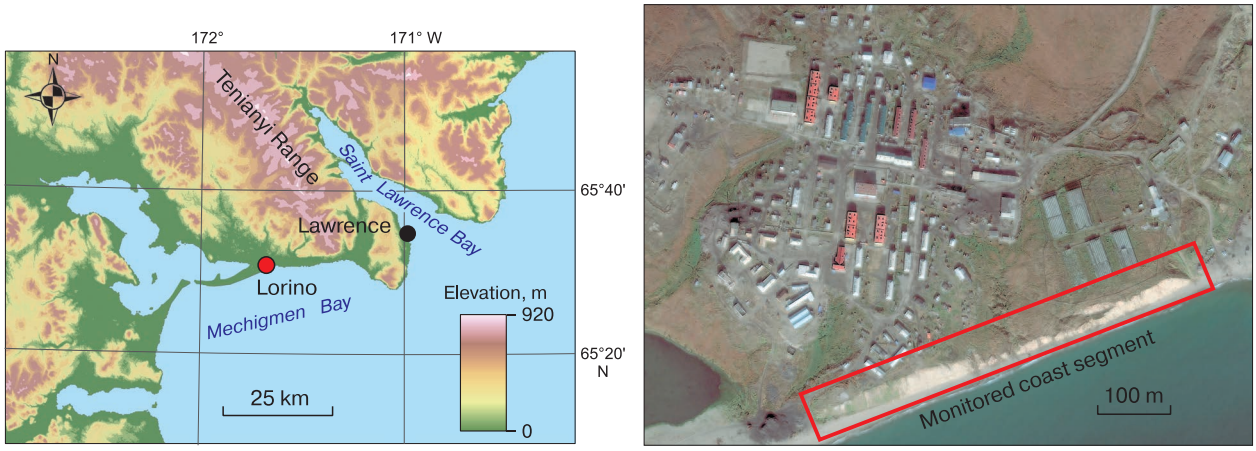

Fig. 1. Location map.

600 m and –9 °C on hill tops farthest inland and 100 m and –4 to –6 °C on lowlands near the sea shore [*Afanasenko et al., 1989; Kolesnikov and Plakht, 1989*].

Lorino is the principal monitoring site of coastal retreat. The coast at the site is exposed to abrasion, like nearly 80 % of the Chukchi Peninsula coast length, and the data from the site are thus well representative [*National Atlas of Russia, 2018*]. The shoreline is straight, NE striking, and open to south- and southeastward waves from both the Arctic and Pacific oceans, as the Aleutian and Commander Islands make poor protection from the Pacific waves. The continental slope has a uniform wave-affected topography with a typical dynamically balanced profile [*Maslakov and Kraev, 2016*].

The coast within the monitoring site is a 750 m long erosional bluff, which is a remnant of a Middle-Upper Pleistocene low marine terrace (II^3–III^1) rising 22–25 m above the sea level. The bluff is a steep bare debris slope, with a nearly vertical outcrop of unfrozen rocks in the upper part. The site includes a thermal erosion gully in the central part, where the surface subsides to 10 m, and a landslide terrace in the east (Fig. 2). Mean annual permafrost temperature varies from –3.4 to –4.8 °C at a depth of 10–15 m; no frozen ground was encountered on the beach above the 10 m depth [*Kraev et al., 2011*]. According to GPR data, the seasonal thaw depth within the developed area varies form 1.0 to 3.5 m, or 1.8 m on average [*Tregubov et al., 2017*]. The coast is composed of frozen Late Pleistocene–Holocene fine-grained marine and glacial-marine deposits. The lithologies are described below with reference to data by *Ivanov* [*1986*] and to engineering geological surveys [*Kraev et al., 2011*] (Fig. 3).

Dark gray stiff clay silt (*9* in Fig. 3) was stripped by drilling on the beach at 1.5–8.5 m below the sea level and was found exposed at the section base (1.5–2.0 m above the sea level) in 2012–2016. The main terrace section to a depth of 0.5–1.0 m below the surface consists of outsize sand, locally with pebble and thin gravel layers (Mechigmen (m II^3) and Krestovsky (f II^4) Fms.), and buried alluvium [*Ivanov,*

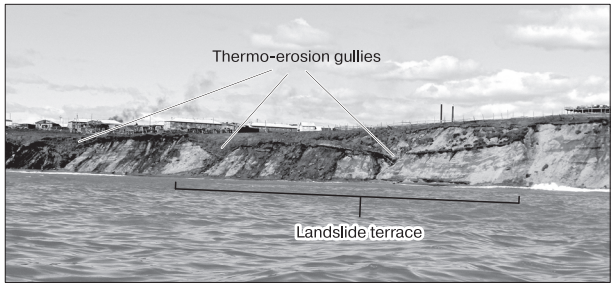

Fig. 2. Landslide terrace and thermo-erosion gullies on the coast at Lorino site. Photograph by A. Maslakov, 2012.

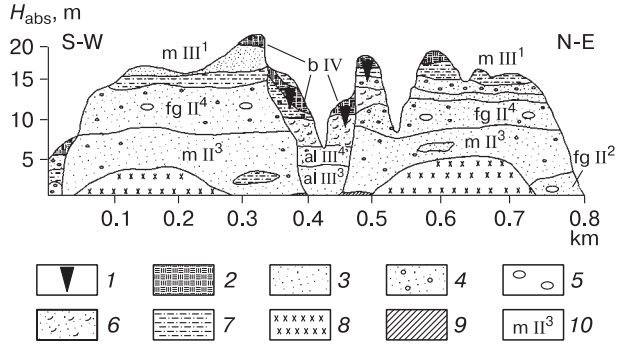

Fig. 3. Geological section across coastal bluff, Lorino site, modified after [*Ivanov, 1986*].

1 – ice wedge (sketch image); *2* – peat; *3* – sand; *4* – sand with pebble and debris; *5* – boulders; *6* – sand with plant detritus; *7* – silt; *8* – talus; *9* – clay silt/clay; *10* – sediment age and genesis. H_{abs} is coast elevation above sea level, m.

1986]. Gray fine sands occur as layers and lenses within a sequence of gray and yellowish-gray medium and coarse sand with sporadic pebble. The visible sediment thickness in boreholes and outcrops reaches 15 m; the section base locally descends below the sea table [*Kraev et al., 2011*]. In the central part of the site, these deposits are buried under saline ice-rich fine sand with plant detritus (*6* in Fig. 3) found as lenses within the 4.0–6.0 m depth interval. The terrace surface is composed of peat and silt (*2* and *7* in Fig. 3) covered with a fill pad within the developed area. Peat is brown in color and encloses silt lenses (up to 30–40 %); its thickness reaches 4 m in the area of gullies at the site center. Below the 0.5–1.0 m depth, there are 1.5–3.0 m high Holocene ice wedges in the middle of the peat outcrop, inserted into silt with their lower ends [*Vasil'chuk et al., 2018*]. Ice in the wedges is clear, sometimes opaque, and encloses vertically oriented air bubbles. The silt (0.5–1.3 to 2.5–5.0 m below the surface) is gray, ice-rich, saline, with 10–30 % of gravel. The fill pad consists of gravel and pebble with silt cement.

The bluff foot is buried under stacked debris of thawed rocks which form a cover over the permafrost. The debris covers the terrace wall to the height of 6–8 m above the sea level and locally buries and preserves coastal snowpacks.

The beach (1.5 m above the water table) is composed of unfrozen yellowish-brownish outsize sand with pebble. It is a 7–10 m wide strip between the sea and the bluff, which is flooded during storm and surge events and thus exposed to the action of waves.

Ice contents vary from 10 to 100 %, according to facies heterogeneity, and generally decrease depthward. The percentages of ice are the highest (50–65 %) in peat and peaty silt, between 20 and 40 % in silt, fine sand, and organic-bearing sand, as low as 15 to 30 % in coarse sand and sand with abundant pebbles, and the lowest (10–15 %) in outsize sands and clay silt (loam) at the section base. The average ice contents estimated in core samples [*Kraev et al., 2011*] are 23–24 % in the western and eastern parts of the bluff and 42 % in the center. Sands have massive cryostructure; ice occurs as small (within 3 mm thick) ice lenses in clay silt and silt and as horizontal or less often vertical lenses (up to 10 cm thick) in peat. Ice wedges (mainly in peat), increase the total ice richness in the central part of the monitored coast.

METHODS

The coastal retreat (landward displacement of the bluff upper and lower edges) was studied using archived old topographic maps of the site area [*Kraev et al., 2011*], a high-resolution (0.5 m) *GeoEye* image of 2010, and geodetic survey data of 2012, 2013, 2014 and 2017 (end of the summer season) performed by the author in the conventional coordinate system. The topographic maps of Lorino after the surveys of 1967, 1979 and 1992 were overlaid on the satellite image in *ArcGIS*, and the positions of the bluff top and foot, as well as the erosion framework, were then digitized. The image was tied to maps with reference to the corners of the preserved buildings, which allowed reducing uncertainty in the satellite image without orthorectifying.

The field geodetic data were superposed over the obtained mosaic. Statistical analysis was performed in *MS Excel*, with estimation of average values and standard deviations (σ) of variables. The parameters of the retreat were quantified along cross-sections spaced at 15–20 m, and the time series were obtained for each section.

The volumetric material loss was estimated per 1 km of coastline per year, for trapezium-shaped transversal profiles, with the top and base corresponding to the terrace and beach surfaces, respectively. Thus, the eroded material volume was found as

$$V_i = \frac{(TD_i + TA_i)h_i}{2},$$

where V_i is the volumetric erosion along the i-th section, m^3 per linear m of the coast; TD_i is the landward displacement of the bluff top, m; TA_i is the landward displacement of the bluff foot, m; h_i is the bluff height above the beach surface, m. This is a simplified formula, without regard to ice content and presence of ground ice (ice wedges). Therefore, it is applicable to ice-poor coasts with mainly pore ice. For this reason, calculations were made for the western and eastern parts of the site, while data for two sections in the center, where erosion includes a thermal erosion component (gullies), were excluded. The amount of erosion between the sections was estimated by interpolation from the next sections.

Proceeding from field observations, the mechanism of coastal retreat at the site can be presented as follows. During the warm season, snowpacks melt down near slopes and frozen sediments of the bluff thaw and become shed down to its foot: coarse-grained sands crumble while peat and peaty silt roll down in lumps. Fans of gullies and minor erosion cut-out provide additional inputs of material. The unfrozen material becomes removed during large surges and storms leaving the frozen rocks exposed. Prolonged wave effects may produce shallow wave-cut niches. Ground ice in the site center is an important agent: it locally accelerates the retreat rate while melting, creates sediment deficit on the submerged continental slope, and liquefies ice-bearing sediments making them flow down to the bluff foot. Thus, sea waves interact with the coast and erode the unfrozen bluff.

The contributions of thermo-abrasion and thermo-denudation (*TA* and *TD*, respectively) were esti-

mated via the normalized difference thermo-erosion index (*NDTI*) [*Günther et al., 2012*]:

$$NDTI = \frac{TD - TA}{TD + TA},$$

where *TD* is the landward movement of the bluff upper edge, mainly by thermal denudation; *TA* is the landward movement of the bluff lower edge, mainly by thermal abrasion. The displacement of the upper edge depends on the rate of material loss from the lower edge, but ice-bonded permafrost exposed by strong erosion preserves relatively steep bluff wall. The *NDTI* values are bracketed between –1 and +1. The ratio is positive when the coast retreat results mainly from thermal denudation and negative when thermal abrasion is the dominant process (Fig. 4).

The sensitivity of coast retreat rates to coast geometry and mechanic strength of thawed and frozen rocks was estimated using normalized erodibility coefficient (*N*). This coefficient is found from strength index of erodibility (K_{st}), which is the volume of rocks transported by unit energy (1 J) of water flow [*Yershov, 1985*].

The parameter K_{st} is commonly found in the field by the penetration method, which is poorly applicable to permafrost, while measurement results may vary broadly within a single sample as a function of cryostructure and properties of soil. K_{st} correlates at $R^2 = 0.98$ with the yield strength (R_{ys}) of rocks [*Yershov, 1985*]:

$$K_{st} = \frac{10^{-3}}{R_{ys}}. \quad (1)$$

For non-saline rocks, without internal friction, R_{ys} can be assumed equal to infinitely long cohesion (C_∞). Otherwise, a correction is applied as [*Vyalov, 1959*]:

$$R_{ys} = C_\infty M. \quad (2)$$

This coefficient depends on the internal friction angle φ, which, in its turn, depends on porosity taken as tabulated values [*Building Norms and Regulations, 2011*]:

$$M(\varphi) = 0.0006\varphi^2 - 0.0463\varphi + 1.0056. \quad (3)$$

The properties of permafrost at the Lorino site remain poorly constrained, in spite of engineering-geological surveys. Therefore, C_∞ in (2) was borrowed from published results of laboratory tests on a large number of samples with different properties [*Vyalov, 1959; Aksenov, 2008*]. Thus, the equation for K_{st} becomes

$$K_{st} = \frac{10^{-3}}{C_\infty M(\varphi)}. \quad (4)$$

The temperature of rocks was assumed to be about 0 °C given that erosion leads to exposure of permafrost and its interaction with air and >0 °C water.

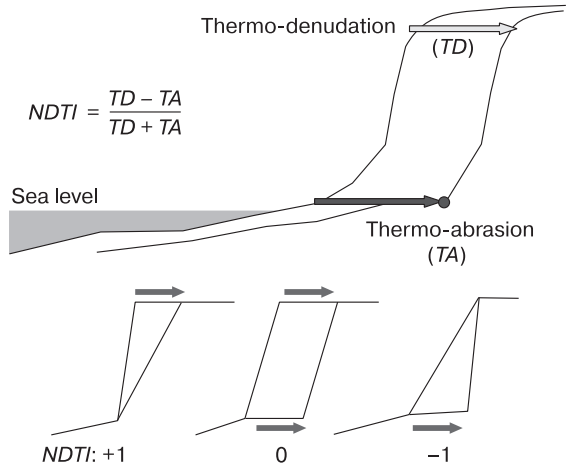

Fig. 4. Landward movement of the upper and lower edges of the coastal bluff by thermodenudation (*TD*) and thermoabrasion (*TA*), respectively. The contributions of the two processes are expressed via the normalized difference thermo-erosion index (*NDTI*) [*Günther et al., 2012*].

The estimated K_{st} values for thawed rocks of different lithologies and grain sizes are:

$0.162 \cdot 10^{-6}$ m^3/J for clay silt, $1.113 \cdot 10^{-6}$ m^3/J for silt, and $(5.568–10.911) \cdot 10^{-6}$ m^3/J for sands. The value $N = 2 \cdot 10^{-5}$ m^3/J for pure ice and peat is assumed proceeding from expertise because estimating their C_∞ value (equation (2)) is impossible.

The total erodibility of coastal rocks within each section is normalized in order to bring the abstract variable K_{st} to specific natural conditions:

$$N_a = \sum_{i=1}^{n} K_{st\,i} \frac{h_i}{h}, \quad (5)$$

where N_a is the erodibility for each section, m^3/J; *n* is the number of layers in the section; $K_{st\,i}$ is the strength index of erodibility for rocks in the *i*-th layer; h_i/h is the thickness of the *i*-th layer normalized to the total section height *h*. Thus, N_a is actually a weigted mean erodibility over the whole section.

The coefficient N_a was divided by the sum of bluff height and beach width in order to account for the effect of coast geometry on retreat rates, because the larger the coast, the slower its retreat [*Vilner, 1955; Kachugin, 1959*]:

$$N = \frac{N_a}{h + d}, \quad (6)$$

where *N* is the normalized erodibility for each section, with regard to coast geometry, m^2/J; *h* is the bluff height, m; *d* is the beach width, m.

Thus, the normalized erodibility for each section is

$$N = \frac{\sum_{i=1}^{n} K_{st\,i} (h_i/h)}{h + d}. \quad (7)$$

This variable has the dimension [m^2/J] or [$m^3/(J \cdot m)$], which physically means the volume of material transported by a flow with the energy 1 J, correlated with the total bluff height and beach width.

Equations (1)–(7) provide a relatively straightforward algorithm for conversion of the parameters of unfrozen and frozen soils estimated by the conventional engineering geological surveys to a parameter that refers to coast vulnerability to erosion. This approach was tested earlier [*Maslakov and Kraev, 2016*], and good fit was obtained between calculated *N* values and measured coastal retreat rates.

RESULTS

Space-time variations in coastal retreat rates

The average coastal retreat at the site was 17 m from 1967 to 2014, at a rate of 0.36 m/yr [*Maslakov and Kraev, 2016*]. Field geodetic surveys in 2017 provided updates for the current coastal dynamics: the retreat was 12.6 m on average for 2014–2017, and the total width of coast eroded between 1967 and 2017 reached 29.6 m. Thus, the retreat for three past years was 43 % of the total value. The retreat rate was within 0.5 m/yr for the first 43 years of monitoring but increased to 1 m/yr from 2010 to 2012, exceeded 2 m/yr in 2012–2014, and amounted to 4.2 m/yr between 2014 and 2017, or almost nine times the initial value (Table 1; Fig. 5). The progressive acceleration of coastal retreat was concurrent with beach shrinking, which reduced from 24 m in 2010 to 7.7 m in 2017. Thus, there have been two stages in the coastal dynamics for the time of monitoring: relatively slow retreat from 1967 to 2010 and rapid retreat since 2010.

Fig. 5. Coast segment at Lorino site that has retreated for fifty years (1967–2017).

1 – coast edge in 2017; *2* – coast edge in 1967; *3* – section and its number. *GeoEye* image, 2010.

In addition to variations in time, the coastal dynamics has been variable in space. The western part of the site (sections 1–19) is as high as 22–25 m above the sea level and is occupied by residential buildings of Lorino community. The bluff is a talus slope composed of outsize sand with enclosed pebble and debris. The beach is 7.7 m wide on average (the beach width is quoted herebelow for 2017). The retreat rate within this coast segment has been relatively slow: a total retreat of 18.1 m for 50 years, at 0.36 m/yr on average, mainly by erosion of thawed talus. The coastal dynamics within this segment has several controls: large bluff height which provides abundant inputs of material to the beach and submerged slope for the given wave energy and slow retreat; relatively low ice content; enclosed gravel and pebbles which accumulate on the beach and protect the shore against wave action.

The central coast segment (sections 20–21) has an elevation of 10–18 m asl (14 m on average) and an average beach width of 5.5 m. The bluff outcrop exposes peat, peat-bearing silt, outsize sand, and clay silt at the base. In its upper part, the bluff encloses ice wedges, up to 5 m wide and 1.5–3.0 m of visible thickness. The segment is cut by several gullies produced by thermal erosion, which accommodate fans of fine

Table 1. **Rate of coastal retreat at Lorino site and its change from 1967 to 2017, modified after [*Maslakov and Kraev, 2016*]**

Period (duration)	Retreat, m	RMSD, m	Retreat rate, m/yr	Reference data
1967–1979 (12 yrs)	2.3	3.0	0.19	Archive maps
1979–1992 (13 yrs)	4.4	3.5	0.34	Archive maps
1992–2010 (18 yrs)	3.5	4.7	0.17	Archive maps and satellite imagery
2010–2012 (2 yrs)	2.0	4.0	1.0	Satellite imagery and field geodetic surveys
2012–2013 (1 yr)	2.3	2.0	2.3	Geodetic surveys
2013–2014 (1 yr)	2.6	2.7	2.6	Geodetic surveys
2014–2017 (3 yrs)	12.6	10.0	4.2	Geodetic surveys
Whole period 1967–2017 (50 yrs)	**29.7**	**14.1**	**0.6**	All data

material transported from the watershed. The retreat patterns are affected by high ice contents and by presence of ice wedges and peat. As a result, the amount of sediment transport is limited and the beach is narrow, making poor protection against surge and storms; the same factors are favorable for the formation of gullies. The segment was excluded from further calculations of coastal dynamics because its retreat has been due to thermal erosion more than to the wave action.

The eastern part of the site (sections 22–35) has an elevation of 18–20 m asl and an average beach width of 7.7 m. The bluff exposes outsize sands and a fragmentary outcrop of gray clay silt at the foot. The coast upper edge is flat; the total retreat from 1967 to 2017 was 42.6 m, at a rate of 0.85 m/yr, or twice the respective values for the western part. The reason may be in finer grain sizes of sediments (smaller amounts of pebble and high percentages of fine sand) and a lower bluff height than in the west, as well as in the presence of erosion cutout and a landslide terrace (Fig. 2).

Generally, the variability of coastal retreat patterns can be expressed via the normalized erodibility coefficient *N* [*Maslakov and Kraev, 2016*], which accounts for geomorphic heterogeneity of different coast segments and erosion strength of rocks exposed in the bluff.

Volumetric erosion

High-resolution topographic surveys of the bluff upper and lower edges run by the author in 2014 and 2017, as well as topographic maps of 1992 and a *GeoEye* image of 2010, allowed estimating the amount of material shed to the sea and the contributions of thermal denudation and thermal abrasion to the coastal retreat.

Table 2. **Coastal erosion rate at Lorino site for 1992–2017**

Period	Volumetric erosion per 1 km of coastline, 1000 m^3/(km·yr)	
	Western segment	Eastern segment
1992–2010	4.78 (±3.49)	–
2010–2014	27.8 (±18.2)	43 (±12.3)
2014–2017	–	101.4 (±30.4)
2010–2017 (whole coast segment at the site)	46.5 (±26.4)	

Note: numerals in braces are RMSD values.

Figure 6 shows the positions of the bluff top and foot in 1992 through 2017, and the material loss for 2010–2017 for each section. Average volumetric erosion was 46.5(±26.4)·1000 m^3/(km·yr), or 46.5 m^3 from each coastline meter per year. In total, about 351 000 m^3/yr of material was shed into the sea from the whole site between 2010 and 2017. See Table 2 for more detail. The calculations were performed for the bluff only, without the beach.

Thermal denudation vs. thermal abrasion

The *NDTI* ratio, which rerfes to the relative contirbutions of thermal denudation and thermal abrasion during coastal retreat, was calculated for the period 2010–2017. Its average over that period was –0.18, which means that the contribution of abrasion was slightly greater than that of denudation (the bluff lower edge retreats faster than the upper one). However, the ratio varies markedly from section to section: from –1.0 to +0.3; abrasion predominates (*NDTI* < 0) in the western part of the site (Fig. 6, *A*) while the contribution of denudation is greater (*NDTI* > 0) in the eastern part (Fig. 6, *B*).

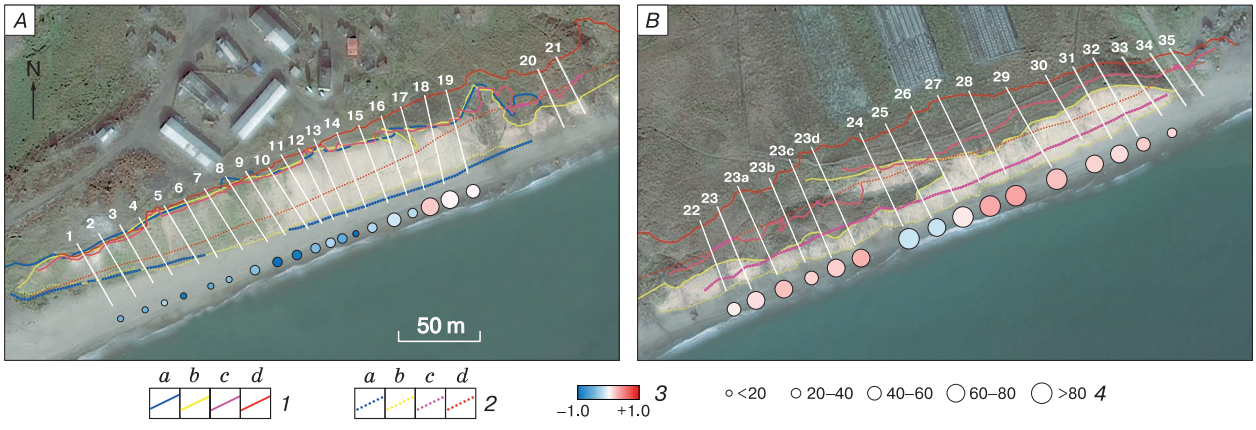

Fig. 6. Slope edge and lower edge at Lorino site in 1992 through 2017, volumetric erosion for 2010–2017 and *NDTI* for western (*A*) and eastern (*B*) coast segments.

1 – upper edge: in 1992 (*a*), 2010 (*b*), 2014 (*c*), 2017 (*d*); *2* – lower edge: 1992 (*a*), 2010 (*b*), 2014 (*c*), 2017 (*d*); *3* – *NDTI*; *4* – erosion rate [1000 m^3/(km·yr)] from 2010 to 2017. Based on *GeoEye* image.

DISCUSSION

Coastal dynamics: causes of change

Acceleration of coastal retreat may be due to climate warming and the ensuing sea ice decline, in the Arctic as a whole and in the Bering Sea in particular, which leaves the coastline more extensively exposed to storm events [*ACIA, 2005; Comiso et al., 2008; Stroeve et al., 2014; Johnson and Eicken, 2016*]. The winter sea-ice coverage in the Bering Sea in 2005–2015 declined for 37 % with respect to that in 1985–1995 [*Ice Contents in Arctic Seas, 2018*]. The Arctic sea ice extent in the 2000–2010s was the lowest over the whole period of instrumental surveys [*Forbes, 2011; Barber et al., 2017*], and the ice-free season has increased correspondingly. As a result, the wave action led to more rapid destruction of coast in many Arctic areas [*Jones et al., 2009; Gusev, 2011; Overeem et al., 2011; Kizyakov et al., 2013; Günther et al., 2015; Farquharson et al., 2018; Gavrilov and Pizhankova, 2018*].

In the East Chukchi part of the Bering Sea coast, erosion is mostly due to lengthening of the open water season in fall and winter months (October–December), when winds are the strongest [*Zimich, 2002; Atkinson, 2005*]. It is the frequency of storms during the ice-free season that is much more important for ice-poor coasts [*Are, 2012*], than air and water temperature changes, unlike the setting in previous years when the coast was covered with ice and the destructive effect of wind action was negligible.

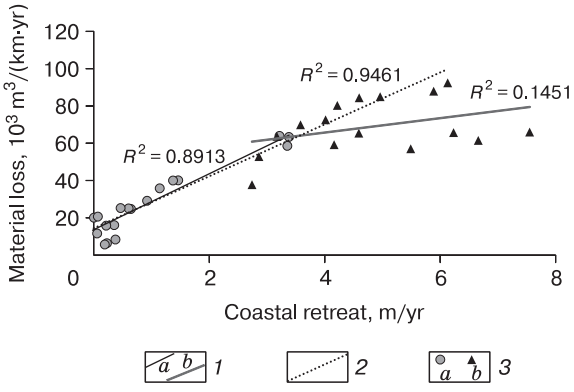

Fig. 7. Rates of coast edge retreat vs. volumetric erosion in sections at Lorino site for 2010–2017.

1 – trends for western (*a*) and eastern (*b*) segments of coastal site; *2* – trend for whole coast at the site without landslide terrace segment (sections 22–24); *3* – rates of coast edge retreat vs. amount of erosion in western (*a*) and eastern (*b*) sections.

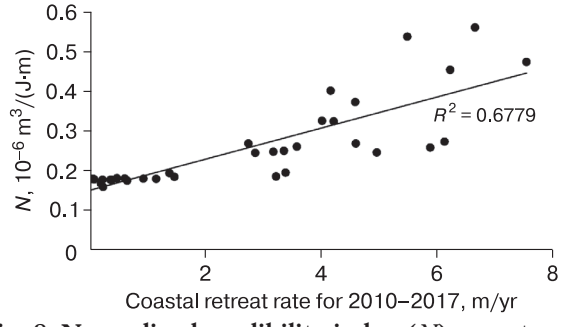

Fig. 8. Normalized erodibility index (*N*) vs. rates of coastal edge retreat for 2010–2017.

Contributions of destructive processes to coastal retreat

The *NDTI* values correlate with volumes of material loss at the Lorino site for 2010–2017, calculated for the monitoring sections: volumetric erosion is greater when thermal denudation is the dominant process. The retreat rate and material loss are moderate in the western part of the Lorino site where abrasion predominates, and are higher in the eastern part mostly subject to denudation (Fig. 6).

Coastal retreat vs. geomorphic and cryological factors

It appears interesting to correlate the measured retreat rates with the coast geometry parameters (bluff height and beach width), volume of material shed into the sea, and erodibility. The volume of erosion products is proportional to retreat rate (Fig. 7). The latter would be expected to be lower at greater bluff height and beach width, but the correlation is poor, though negative (Table 3). The reason may be in uneven distribution of ice and facies heterogeneity of exposed rocks which are expressed in the erodibility *N* showing a strong correlation with retreat rates: $R = 0.82$ (Fig. 8).

However, the correlation is poor within the segment of the landslide terrace: the correlation coefficient (R^2) is 0.15 with the landslide zone included into calculations and 0.82 without it (Fig. 7), according to points below the approximation line (*3b* in Fig. 7).

With this approach, the greater contribution of thermal denudation within more rapidly retreating coast segments appears reasonable (Fig. 6). The displacement of the lower edge of the bluff is limited by the permafrost-beach junction (or by the depth of thermo-niches) during storms and by the natural bluff slope, whereas the bluff's upper edge (used com-

Table 3. **Geomorphic and predicted indicators of coastal dynamics and retreat rates along sections at Lorino site for 2010–2017, compared**

Parameter	Bluff height	Beach width	Erosion value*	*N*
Correlation (*R*) of variables with coastal retreat in sections	–0.54 (*n* = 37)	–0.23 (*n* = 37)	0.89 (*n* = 35)	0.82 (*n* = 35)

*Coastal retreat vs. erosion volume correlation was calculated including the landslide terrace segment.

Note: *n* is number of sections included into calculations.

monly to estimate the retreat rate) can undergo greater displacement, for instance, in the case of cryogenic landsliding or formation of gullies and terraces by thermal erosion.

Note also that the correlation of erodibility with retreat rates is higher for 2010–2017 (Table 3) than for 2010–2014 (0.782) [*Maslakov and Kraev, 2016*], possibly, because the effect of random events attenuates over longer periods of observation.

CONCLUSIONS

Space and time variations in the rate of coastal retreat observed at the Lorino monitoring site allow the following inferences.

1. Coastal retreat at the site for three past years (2014–2017) became at least ten times faster than in the previous fifty years between 1967 and 2010: 4.2 m/yr against 0.17–0.34 m/yr, as a result of ice-free season lengthening and enhanced wave action on the coast. The retreat for 50 years has been twice smaller in the western part of the site than in the east: 18.1 m against 42.6 m.

2. The *NDTI* distribution shows that thermal abrasion predominates over thermal denudation in the western part while the contribution of denudation is greater in the east. The presence of gullies and a rapidly eroded landslide terrace in the eastern flank maintains more rapid retreat of the bluff top.

3. The amount of material shed annually into the sea between 2010 and 2017 at the Lorino site (without the beach deposits) reached ~35,000 m^3.

4. The normalized erodibility *N*, which allows for the coast geometry and erosion strength of sediments, correlates well with retreat rates at the site for the period between 2010 and 2017 ($R = 0.82$), and the correlation is higher than for the shorter period from 2010 to 2014 ($R = 0.78$). Therefore, geomorphic and cryological factors are important agents in coastal retreat in the current conditions of strong wave action on the coast. The suggested algorithm for calculating the coefficient *N* is applicable to estimation of retreat rates at sites of economic development where sediments with different ice contents and compositions are exposed to storms.

I wish to thank G.M. Zelensky, D.G. Zamolodchikov, G.N. Kraev, and E.V. Antonov for assistance in the field. The manuscript profited much from constructive criticism by V.E. Tumsky and E.I. Pizhankov.

The study was supported by grant OPP-0352957 from the U.S. National Science Foundation (for several field campaigns) and by grant 18-05-60300 from the Russian Foundation for Basic Research.

References

ACIA, 2005. Arctic Climate Impact Assessment. Cambridge, Cambridge University Press, 1042 pp.

Afanasenko, V.E., Zamolotchikova, S.A., Tishin, M.I., Zuev, I.A., 1989. The North Chukchi region, in: Geocryology of the USSR. East Siberia and Russian Far East. Nedra, Moscow, pp. 280–293. (in Russian)

Aksenov, V.I., 2008. Saline permafrost in the Arctic coast as foundation for buildings and structures. All about Construction, Moscow, 340 pp. (in Russian)

AMAP, 2017. Snow, Water, Ice and Permafrost in the Arctic (SWIPA) 2017. Arctic Monitoring and Assessment Programme (AMAP), AMAP, Oslo, 269 pp.

Are, F.E., 2012. Erosion of Arctic Coastal Plain. Geo Publishers, Novosibirsk, 291 pp. (in Russian)

Atkinson, D.E., 2005. Observed storminess patterns and trends in the circum-Arctic coastal regime. Geo-Marine Letters 25 (2–3), 98–109.

Barber, D.G., Meier, W.N., Gerland, S., 2017. Arctic sea ice, in: Snow, Water, Ice and Permafrost in the Arctic (SWIPA) 2017. Arctic Monitoring and Assessment Programme (AMAP), AMAP, Oslo, pp. 103–136.

Belova, N.G., Shabanova, N.N., Ogorodov, S.A., 2017. Erosion of permafrost coasts of Kara Sea near Kharasavey Cape, Western Yamal. Earth's Cryosphere (Kriosfera Zemli) XXI (6), 73–83.

Building Norms and Regulations, 2011. Working Document SP 22.13330.2011. Basements and Foundations (Actual Edition SNiP 2.02.01-83). Minregionrazvitiya RF, Moscow, 155 pp. (in Russian)

Chukchi Municipal Area, Chukchi Autonomous District (Okrug), Official website. – URL: www.chukotraion.ru (submittal date: 30.11.2017).

Comiso, J.C., Parkinson, C.L., Gersten, R., Stock, L., 2008. Accelerated decline in the Arctic sea ice cover. Geophys. Res. Lett. 35 (1), DOI: 10.1029/2007GL031972.

Farquharson, L.M., Mann, D.H., Swanson, D.K., Jones, B., Buzard, R.M., Jordan, J.W., 2018. Temporal and spatial variability in coastline response to declining sea-ice in northwest Alaska. Marine Geology 404, 71–83, DOI: 10.1016/j.margeo.2018.07.007.

Forbes, D.L. (Ed.), 2011. State of Arctic Coast 2010 – Scientific Review and Outlook. IASC, LOICD, AMAP, IPA. Helmholtz-Zentrum Geesthacht, Geesthacth, 170 pp.

Gavrilov, A.V., Pizhankova, E.I., 2018. Dynamics of permafrost in the coastal zone of Eastern-Asian sector of the Arctic. Geography, Environment, Sustainability 11(1), 20–37.

Grigoriev, M.N., Razumov, S.O., Kunitskiy, V.V., Spektor, V.B., 2006. Dynamics of the Russian East Arctic Sea coast: major factors, regularities and tendencies. Kriosfera Zemli X (4), 74–94.

Günther, F., Overduin, P., Sandakov, A., Grosse, G., Grigoriev, M.N., 2012. Thermo-erosion along the yedoma coast of the Buor Khaya Peninsula, Laptev Sea, East Siberia. Proc. 10th Intern. Conf. Permafrost, Salekhard, Russia, Volume 1, pp. 137–142.

Günther, F., Overduin, P.P., Yakshina, I.A., Opel, T., Baranskaya, A., Grigoriev, M.N., 2015. Observing Muostakh disappear: permafrost thaw subsidence and erosion of a ground-ice-rich island in response to arctic summer warming and sea ice reduction. Cryosphere 9, 151–178.

Gusev, E.A., 2011. Observations of geomorphological processes in northern West Siberia (case study of Sopochnaya Karga). Uspekhi Sovrem. Estestvoznaniya, No. 9, 19–22.

Ice Contents in Arctic Seas, 2018. Data over 10-day and monthly cycles, according to SSMR-SSM/I (NASATEAM algorithm). – URL: http://www.aari.ru/resources/d0021_22/_d0022.php (submittal date: 29.03.2018).

Irrgang, A.M., Lantuit, H., Manson, G.K., Günter, F., Grosse, G., Overduin, P.P., 2018. Variability in rates of coastal change along the Yukon coast, 1951 to 2015. J. Geophys. Res. Earth Surface 123 (4), 779–800, DOI: 10.1002/2017JF004326.

Isachenko, A.G., 1985. Landscapes of the USSR. Leningrad University Press, Leningrad, 320 pp. (in Russian)

Ivanov, V.F., 1986. Quaternary Deposits in the Eastern Chukchi Coast. DVNTC AN SSSR, Vladivostok, 140 pp. (in Russian)

Johnson, M., Eicken, H., 2016. Estimating Arctic sea-ice freeze-up and break-up from the satellite record: A comparison of different approaches in the Chukchi and Beaufort Seas. Elementa: Science of the Anthropocene, No. 4, 000124, DOI: 10.12952/journal.elementa.000124.

Jones, B.M., Arp, C.D., Jorgenson, M.T., Hinkel, K.M., Schmutz, J.M., Flint, P.M., 2009. Increase in the rate and uniformity of coastline erosion in Arctic Alaska. Geophys. Res. Lett. 36, L03503.

Kachugin, E.G., 1959. Engineering geological surveys and prediction of shoreline retreat in water reservoirs, in: Recommendations for Studies of Erosion in the Shores of Water Reservoirs. Gosgeoltekhizdat, Moscow, pp. 3–89. (in Russian)

Kizyakov, A.I., Zimin, M.V., Leibman, M.O., Pravikova, N.V., 2013. Monitoring of the rate of thermal denudation and thermal abrasion on the western coast of Kolguev Island, using high resolution satellite images. Kriosfera Zemli XVII (4), 36–47.

Kobysheva, N.V., 2001. Climate of Russia. Gidrometeoizdat, St. Petersburg, 654 pp. (in Russian)

Kolesnikov, S.F., Plakht, I.R., 1989. The Chukchi region, in: Popov, A.I. (Ed.), Regional Permafrost Studies, Moscow University Press, Moscow, pp. 201–217. (in Russian)

Kraev, G.N., Maslakov, A.A., Grebenets, V.I., Kalanto, N.L., 2011. Engineering-geocryological problems in territories populated by indigenous peoples of the East Chukchi Peninsula. Inzh. Geologiya, No. 9, 52–57.

Kritsuk, L.N., Dubrovin, V.A., Yastreba, N.V., 2014. Results of complex study of the Kara Sea shore dynamics in the area of the meteorological station Marre-Sale, using GIS-technologies. Earth's Cryosphere (Kriosfera Zemli) XVIII (4), 52–62.

Lantuit, H., Overduin, P.P., Couture, N., Wetterich, S., Are, F., Atkinson, D., Brown, J., Cherkashov, G., Drozdov, D., Forbes, D., Graves-Gaylord, A., Grigoriev, M., Hubberten, H-W., Jordan, J., Jorgenson, T., Ødegård, R.S., Ogorodov, S., Pollard, W., Rachold, V., Sedenko, S., Solomon, S., Steenhuisen, F., Streletskaya, I., Vasiliev, A., 2012. The Arctic Coastal Dynamics database: a new classification scheme and statistics on Arctic permafrost coastlines. Estuaries and Coasts 35, 383–400, DOI: 10.1007/s12237-0109362-6.

Lantuit, H., Pollard, W.H., 2008. Fifty years of coastal erosion and retrogressive thaw slump activity on Herschel Island, southern Beaufort Sea, Yukon Territory, Canada. Geomorphology 95, 84–102.

Maslakov, A., Kraev, G., 2016. Erodibility of permafrost exposures in the coasts of Eastern Chukotka. Polar Sci. 10, 374–381.

National Atlas of Russia. Book 2. Bering Sea. – URL: http://nacionalnyiatlas.rf/cd2/285-288/285-288.html (submittal date: 19.03.2018).

Overeem, I., Anderson, R.S., Wobus, C.W., Clow, G.D., Urban, F.E., Matell, N., 2011. Sea ice loss enhances wave action at the Arctic coast. Geophys. Res. Lett. 17 (38), L17503.

Pachauri, R.K., Meyer, L.A. (Eds.), 2014. IPCC, 2014: Climate Change 2014: Synthesis Report. Contribution of Working Groups I, II and III to the Fifth Assessment Report of the Intergovernmental Panel on Climate Change. Core Writing Team, IPCC, Geneva, 151 pp.

Parmuzin, S.Yu., 1968. Russian far Northeast, in: Gvozdetsky, N.A. (Ed.), Physiographic Division of the USSR, Nauka, Moscow, pp. 481–503.

Pizhankova, E.I., 2016. Modern climate change at high latitudes and their influence on the coastal dynamics of the Dmitriy Laptev Strait area. Earth's Cryosphere (Kriosfera Zemli) XX (1), 46–59.

Romanovsky, V., Isaksen, K., Drozdov, D., 2017. Changing permafrost and its impacts, in: Snow, Water, Ice and Permafrost in the Arctic (SWIPA) 2017. Arctic Monitoring and Assessment Programme (AMAP), AMAP, Oslo, pp. 65–102.

Stroeve, J.C., Markus, T., Boisvert, L., Miller, J., Barrett, A., 2014. Changes in Arctic melt season and implications for sea ice loss. Geophys. Res. Lett. 41, 1216–1225, DOI: 10.1002/2013GL058951.

Tregubov, O.D., Kraev, G.N., Maslakov, A.A., 2017. Modeling of the permafrost top from GPR data, in: Proc. 13th Conf. "Engineering Geophysics – 2017" (Kislovodsk, 23–28 April 2017). EAGE, Moscow, http://earthdoc.eage.org/publication, DOI: 10.3997/2214-4609.201700389.

Vasil'chuk, Yu.K., Budantseva, N.A., Vasil'chuk, A.C., Maslakov, A.A., Chizhov, Ju.N., 2018. Oxygen isotope composition of Holocene ice wedges in Eastern Chukotka. Doklady Earth Sci. 480 (2), 758–762.

Vilner, B.A., 1955. Features of coastal dynamics in Arctic seas, in: Transactions, Institute of Oceanography, 4, pp. 53–57.

Vyalov, S.S., 1959. Rheology and Bearing Capacity of Permafrost. Izd. AN SSSR, Moscow, 153 pp. (in Russian)

Yershov, E.D. (Ed.), 1985. Laboratory Studies of Permafrost. Moscow University Press, Moscow, 350 pp. (in Russian)

Zimich, P.I., 2002. Strong storms on the Chukchi Coast and their Prediction. SVKNII DVO RAN, Magadan, 177 pp. (in Russian)

Received June 1, 2018
Revised version received September 20, 2018
Accepted October 19, 2018